Characterizing Thermal Performance of Buildings Using Dynamic Model Identification

Geert Bauwens   **Staf Roels**

ABSTRACT

The energy performance of a building is, apart from installed systems and building usage, primarily determined by the thermal characteristics of the building envelope. An important distinction needs to be made between the theoretical building energy performance as calculated in the design phase and its actual as-built performance. Several studies have shown that these can differ rather significantly.

As a first step in bridging this energy performance gap, this paper investigates the possibility of characterizing the as-built thermal performance of building envelopes using dynamic data analysis of appropriate experiments. Essentially, the investigated building is modeled as a simplified thermal system. The parameters governing the workings of the thermal system are estimated by fitting it to measured thermal performance data of the building, by means of maximum likelihood estimation.

A scale model of a building serves as a case study. Identical measurement campaigns are simulated in winter and summer. Models of increasing complexity are fitted to the simulated measurement data of both campaigns. The fitted models are evaluated and compared on the basis of their log-likelihood, output residuals, and corresponding auto-correlation function and the cumulated periodogram. Using likelihood ratio tests, it is assessed whether models of larger complexity perform significantly better than smaller models. The best-performing models of different model orders are cross-validated. Hence, a model order tailored to the investigated fabric, the imposed experiment, and the weather conditions is determined.

INTRODUCTION

Background

The energy performance of a building is essentially determined by the thermal characteristics of the building fabric, the installed services, and the building usage. As the latter is not easily predicted nor controlled, the first two are decisive in achieving the envisaged building energy performance, for both newly built and renovated buildings. An important distinction needs to be made here between the theoretical building fabric thermal performance as calculated in the design phase and its actual as-built performance. Several studies have shown that these can differ rather significantly (Hens et al. 2007; Bell et al. 2010; Lowe et al. 2007). This difference, among others, can be attributed to the applied materials differ-

ing from the designated ones, poor detailing and/or workmanship issues, and physical phenomena such as thermal bridging, wind washing, and air looping. Hence, the thermal performance characterization of a building envelope, as investigated in this paper, constitutes an important step in bridging the gap between the designed and the as-built energy performance of buildings.

Buildings essentially constitute dynamic thermal systems, which can be modeled as a series of thermal nodes (e.g., an indoor air temperature node or a node in the capacitive building fabric, among others). Such nodes, often referred to as *states,* bear a certain capacity (C) to store or release heat and are interlinked through thermal resistances (R). The system dynamics are determined by its time constants (e.g., how fast the indoor air temperature responds when the outdoor air

Geert Bauwens *is a research assistant and **Staf Roels** is a professor in the Building Physics Section, Department of Civil Engineering, KU Leuven, Leuven, Belgium.*

temperature rises with a given step), which directly relate to the heat capacities associated with the thermal nodes and the thermal resistances between them. Depending on the investigated building and the way in which it is excited (e.g., by a specifically designed experiment), its dynamics will be marked by one or more time constants. The aim of this paper is to evaluate the suitability of certain simplified thermal models to grasp the building dynamics, based on the analysis of experiments performed on the building of interest. In a next step, these models can be used to characterize the physical parameters of the building (R and C, among others) or simulate the building behavior, given known boundary conditions or inputs.

The analysis methodology used in this paper is based on a data-driven identification of models with physical relevance, referred to as *grey-box modeling*. Essentially, this holds the middle between white-box modeling, where the thermal behavior is assumed to be known and deterministic, and black-box modeling, in which prior physical knowledge is discarded and the main aim is to describe the output of the thermal system (e.g., indoor air temperature) as a function of the measured input (e.g., outdoor air temperature, solar radiation, etc.).

A grey-box model mathematically describes the investigated building as a simplified thermal system, based on a physical interpretation of that building. The description consists of a system of continuous-time stochastic differential equations and discrete-time measurement equations. As such, the model comprises a certain configuration of parameters (thermal resistances, heat capacities, solar apertures, etc.) that govern the links between temperature nodes in a thermal system. The unknown parameters are then estimated on the basis of information that is embedded in the measurement data, using maximum likelihood estimation (Kristensen and Madsen 2003). The obtained parameter values serve to maximize the probability that, assuming respective models, the measured response is actually observed.

Instead of applying the methodology on a real building, a very simple, small scale model of a building, the Knauf Insulation Test Box (KI Test Box) is used as a case study. This box was designed as an object of study for the Round Robin Experiment organized in the framework of the currently ongoing IEA ECBCS Annex 58 project (Roels 2011). The KI Test Box allows for great control of the experiment conditions, facilitating the investigation of the reliability and practicality of the applied data analysis methods.

Instead of acquiring measurement data by performing real experiments, different measurement campaigns are simulated on the KI Test Box. Experiments are simulated during a winter month (January 2011) and a summer month (July 2011). Both experiments excite the indoor environment of the box using an identical predetermined heating power that is made to exhibit the characteristics of a pseudo random binary signal (PRBS). Hence, the only difference between winter and summer experiments lies in the particular weather conditions.

Grey-box models of increasing complexity are fitted to the simulated measurement data. The performance of the fitted models is compared using statistical methods. More specifically, the model log-likelihoods are compared, likelihood ratio tests (Thyregod and Madsen 2006) are used to assess whether a more complex model performs significantly better than a smaller (less complex) sub-model (Bacher and Madsen 2011), the residuals and corresponding autocorrelation functions (ACFs) are plotted to investigate how well the models are able to predict the response of the building (referred to as the *states*) based on the imposed boundary conditions (referred to as the *inputs*), and finally, the cumulated periodogram serves to test whether the residuals exhibit white noise behavior. A white noise signal represents a sequence of mutually uncorrelated identically distributed random variables with zero mean and constant variance.

Outline

The investigated building scale model and the simulated measurement campaigns are discussed in the section "Simulated Measurement Campaigns." In a following section, the candidate grey-box models are described and the statistical methods to select the most appropriate one are introduced. In the section "Identification of Simulated Box," these models are fitted to the simulated measurement data in winter and summer. A forward selection strategy reveals the most suitable model based on the performance. The best-performing models of consecutive orders are cross-validated. Conclusions are drawn in the last section.

SIMULATED MEASUREMENT CAMPAIGNS

Knauf Insulation Test Box

Instead of applying the methodology on real experiments applied on a real building, a small scale model of a building, the KI Test Box (Figure 1) of IEA ECBCS Annex 58 (Roels 2011), is investigated. The investigated test box has a cubic form, with exterior dimensions of $120 \times 120 \times 120$ cm^3. The floor, roof, and wall components are all identical and exhibit a thickness of 12 cm, leaving an inner volume of $96 \times 96 \times 96$ cm^3. One wall contains a window component with dimensions 60×60 cm^2. The fixed window frame has the same thickness as the other façade elements. A structure is provided around the box that allows it to remain free from the thermal influence of the ground. Hence, the box can be considered as floating in free air.

As such, the test box allows for rather simple, well-controlled experiments to investigate different scenarios and to determine the influence of different aspects that come to play in the thermal behavior of buildings.

Simulation of Test Box

Instead of acquiring measurement data by performing real experiments, different measurement campaigns are simulated, using Physibel software VOLTRA 7.0w (Physibel 2011).
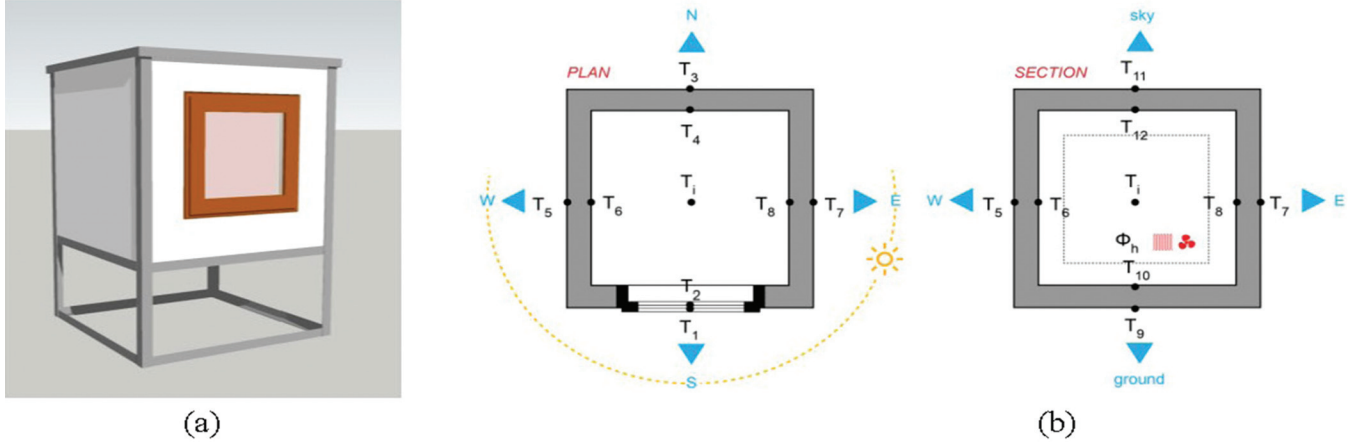
Figure 1 *Investigated test box: (a) three-dimensional picture of simulated test box and (b) plan and section of simulated test box. The numbered nodes, T$_1$, T$_2$, ..., T$_{12}$, refer to the inside (even numbers) and outside (odd numbers) surface temperatures (in the middle of the surface). T$_i$ indicates the air temperature inside the box. Φ_h represents the heating power injected into the indoor environment of the box.*

Table 1 shows the boundary conditions assumed as a basis for the simulations. The simulation time step is 1 min. The thermal conductivity, density, and specific heat of all materials are assumed constant. Inside and outside surface heat fluxes are decoupled in a convective and radiative component. Additionally, the radiative heat exchange to the sky and environment are decoupled. The south-oriented window is modeled as a gas-filled double-glazed window. Ventilation heat losses have not been incorporated in the simulations. The box fabric is assumed perfectly airtight. Hence, this study focuses only on the characterization of the test box with respect to transmission heat losses.

Simulated Experimental Conditions

The test box is simulated to be subjected to measurement campaigns in January 2011 and July 2011. Figure 2 shows the applied heating power signal, the resulting indoor air temperatures, indoor and outdoor surface temperatures, and governing weather conditions (for Limelette, Belgium) during both campaigns. Assuming Equation 1 holds, the sky temperature T_{sky} is calculated from infrared radiation measurements on a horizontal surface $q_{ir,hor}$ (with σ as the Stefan-Boltzmann constant).

$$T_{sky} = \left(\frac{q_{ir,hor}}{\sigma} \right)^{1/4} \qquad (1)$$

As suggested by Rabl (1988), a more sensible assessment of the solar apertures can be obtained when direct and diffuse solar radiation are separated for each of the building's window orientations. The global and diffuse solar radiation on a horizontal surface are available as measured input. In combination with accurate knowledge of the sun position (Reda and Andreas 2008) throughout the experiment, all five projections (horizontal, north, east, south, and west) of the direct solar

radiation in all orientations are calculated. In what follows, $q_{sw,*}$ denotes the global solar radiation projection perpendicular to orientation * (e.g., south).

Applied Excitation Signal

During both measurement campaigns, the KI Test Box is heated with a predetermined power corresponding to a PRBS. The PRBS properties of interest are that it is uncorrelated with the weather conditions and has an autocorrelation that approximates that of white noise (Godfrey 1980).

The PRBS effectively shifts between two levels: full power and no power. The time period λ indicates the shortest time step at which the signal is maintained at a certain level. As suggested by Madsen and Schultz (1993), λ is chosen to closely relate to the smallest expected time constant of the investigated box, and the signal order n may be selected so that $N\lambda = (2^n - 1)\lambda$ closely relates to the largest time constant of the box.

The system is excited using two consecutive PRBSs. The first part is designed in such a way that the system is excited around time constants of 2 h (λ) and 30 h ($N\lambda$). This signal has periods at one level between 2 h and 8 h ($n\lambda$). The second part has a λ of 4 h and $n\lambda$ of 16 h. Hence, the system is excited around time constants of 4 h and 60 h. Both PRBSs are repeated 4 times, resulting in a total experiment duration of 15 days. The parameters governing the heating power signal generation are collected in Table 2. The resulting signal is incorporated in Figure 2a and is identical for both January and July experiments.

Perturbed Simulated Measurement Data

In order to yield the simulated measurement data as more representative, the data are perturbed by adding random noise proportional to the original data (up to ±1%). This effectively

Table 1. Assumed Indoor and Outdoor Boundary Conditions During Simulations

Outdoor Boundary Conditions		
$q_{esc} = h_{ec}(\theta_a - \theta_{es})$	q_{esc}	External surface convective heat flux
	h_{ec}	Variable convective heat transfer coefficient $= 5.85\ v^{0.52}$ (leeward side) $= 7.18\ v^{0.57}$ (windward side)
	θ_a	Ambient air temperature
	θ_{es}	External surface temperature
$q_{esr} = \xi\sigma F_e(T_{es}^{\ 4} - T_{e,rad}^{\ 4})$ $q_{esr,sky} = \xi\sigma F_{sky}(T_{es}^{\ 4} - T_{sky,rad}^{\ 4})$	q_{esr}	External surface radiative heat flux to environment
	$q_{esr,sky}$	External surface radiative heat flux to sky
	ξ	External surface emissivity = 0.9
	σ	Stefan-Boltzmann constant
	T_{es}	Absolute external surface temperature
	$T_{e,rad}$	Average radiative temperature environment
	F_e	Environment view factor
	$T_{sky,rad}$	Average radiative temperature sky
	F_{sky}	Sky view factor
$q_{solar} = \alpha E_{st}$	q_{solar}	Solar irradiation
	α	Solar absorption factor of external surface = 0.97
	E_{st}	Solar radiation on surfaces, cfr. Muneer (1989)
Indoor Boundary Conditions		
$q_{isc} = h_{ic}(\theta_i - \theta_{is})$	q_{isc}	Internal surface convective heat flux
	h_{ic}	Variable convective heat transfer coefficient $= 1.46\ (\theta_i - \theta_{is})^{1/3}$
	θ_i	Internal air temperature (assumed uniform)
	θ_{is}	Internal surface temperature
$q_{isr} = \xi\sigma(T_{is}^{\ 4} - T_{i,rad}^{\ 4})$	q_{isr}	Internal surface radiative heat flux
	ξ	Internal surface emissivity = 0.9
	σ	Stefan-Boltzmann constant
	T_{is}	Absolute averaged internal surface temperature
	$T_{i,rad}$	Average radiative temperature interior room

simulates measurement noise, frequently specified as a percentage of the measured quantity.

SIMPLIFIED MODELING OF THE BUILDING ENVELOPE THERMAL PERFORMANCE

Lumped State-Space Modeling

As mentioned previously, the investigated building is described by a series of simplified thermal systems of varying complexity, referred to as *grey-box models*. All of the candidate models considered in this paper are linear time-invariant and can be mathematically described as a system of continuous-time stochastic differential equations (Equation 2) and discrete-time measurement equations (Equation 3):

$$dT = (AT + BU)dt + d\omega(t) \qquad (2)$$

$$Y_k = CT_k + DU_k + \varepsilon_k \qquad (3)$$

where

T = state vector (response of the KI Test Box, e.g., indoor air temperature)

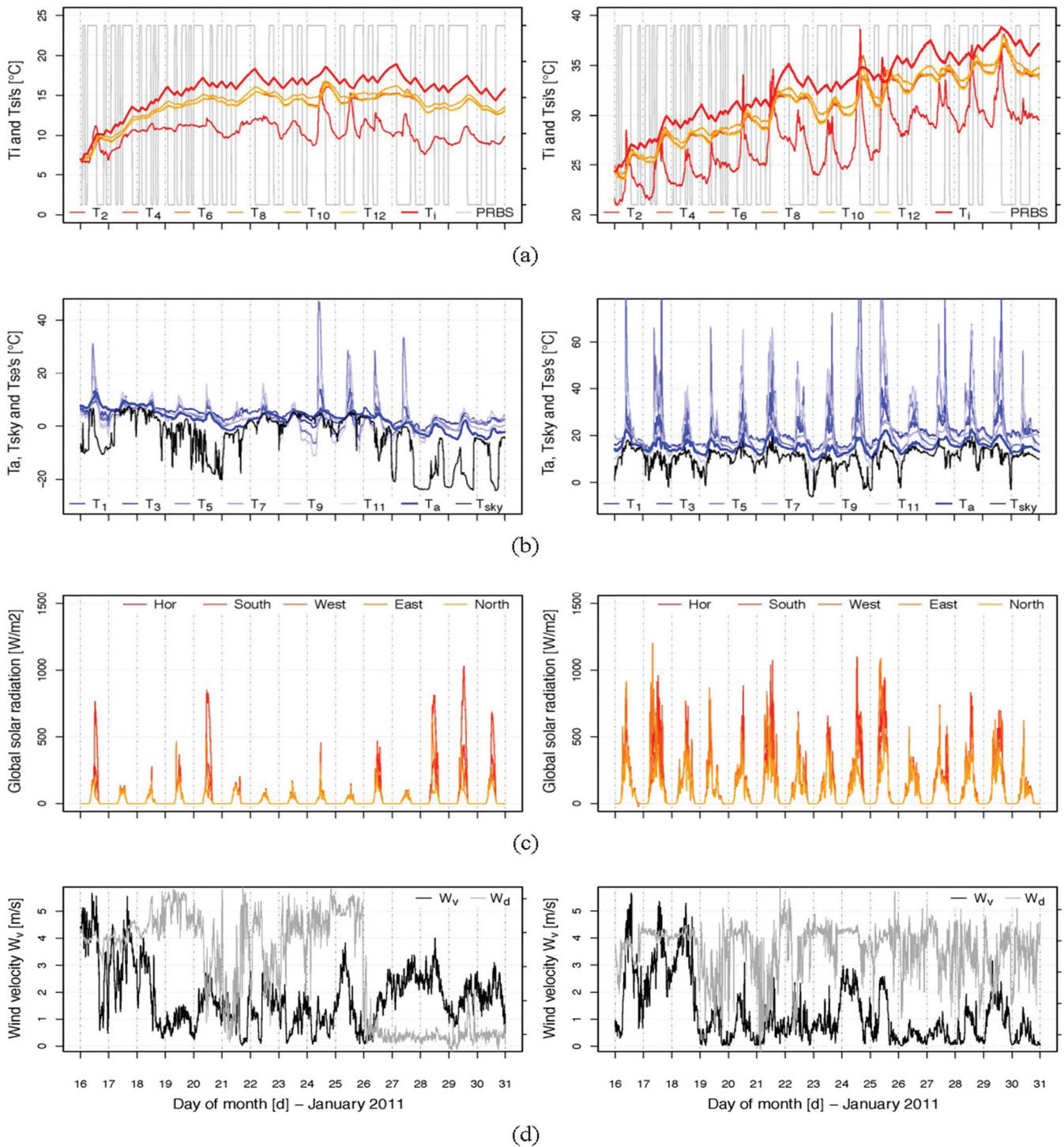U = input vector (e.g., outdoor air temperature, solar radiation, heating power)

Figure 2 *Simulated measurement campaigns in January 2011 (left) and July 2011 (right): (a) simulated indoor air temperature, composite PRBS as heating power, and indoor surface temperatures; (b) measured ambient air temperature, calculated sky temperature, and simulated exterior surface temperatures; (c) measured global solar radiation on horizontal surface and calculated global solar radiation projections; and (d) measured wind speed and direction.*

A, B =   parameter matrices that govern the dynamics of the states and how inputs alter the system, respectively.

Hence, A and B consist of physical parameters that serve to characterize the heat dynamics of the test box and are of particular interest here.

    In this study, depending on the complexity of the considered model, the input vector comprises up to four variables: outdoor air temperature T_a, heating power Φ_h, solar radiation projection $q_{sw,*}$, and sky temperature T_{sky}.

$$U = \begin{bmatrix} T_a & \phi_h & q_{sw,*} & T_{sky} \end{bmatrix}^T \quad (4)$$

    In all of the considered models, the indoor air temperature T_i is considered to be the sole output or response of the system. The candidate models considered in this paper, of increasing complexity, are described in more detail in the following subsections on model Ti, model TiTe, and model TiTeiTea.

Model Ti

    As illustrated in Figure 3a and described mathematically in Equations 5–7, the indoor air temperature T_i [K] is considered the sole state of the system. The outdoor ambient temperature

Table 2. Parameters of PRBS Generation

#	Name	n	λ	N	$n\lambda$	$N\lambda$
4	PRBS1	4	2 h	15	8 h	30 h
4	PRBS2	4	4 h	15	12 h	60 h

T_a (Equations 5–7), the heating power Φ_h (Equations 6–7), and the solar radiation $q_{sw,*}$ (Equation 7) are added consecutively as inputs to the system. The identified heat capacity C_i will, aside from the limited heat capacity associated with the indoor air, include the heat capacity of the building fabric that is effectively excited during the experiment. R_{ia} [K/W] represents the thermal resistance between indoor and outdoor air (Equations 5–7). The fraction of solar radiation that actually constitutes a heat input to the indoor air of the KI Test Box is denoted A_{sw} [m²·K] (Equation 7). In this case, as illustrated in Figure 3a, it includes the fraction entering through the transparent part $A_{sw,t}$ and opaque part $A_{sw,o}$.

Model Ti.1

$$dT_i = \left(\frac{1}{C_i R_{ia}} (T_a - T_i) \right) dt + d\omega_i(t) \quad (5)$$

Model Ti.2

$$dT_i = \left(\frac{1}{C_i R_{ia}} (T_a - T_i) + \frac{\phi_h}{C_i} \right) dt + d\omega_i(t) \quad (6)$$

Model Ti.3

$$dT_i = \left(\frac{1}{C_i R_{ia}} (T_a - T_i) + \frac{\phi_h}{C_i} + \frac{A_{sw} q_{sw,*}}{C_i} \right) dt + d\omega_i(t)$$

$$(7)$$

Model TiTe

    To more accurately take into account the dynamic response of the fabric, second-order models are suggested in Equations 8–10. Essentially, as depicted in Figure 3b, an addi-
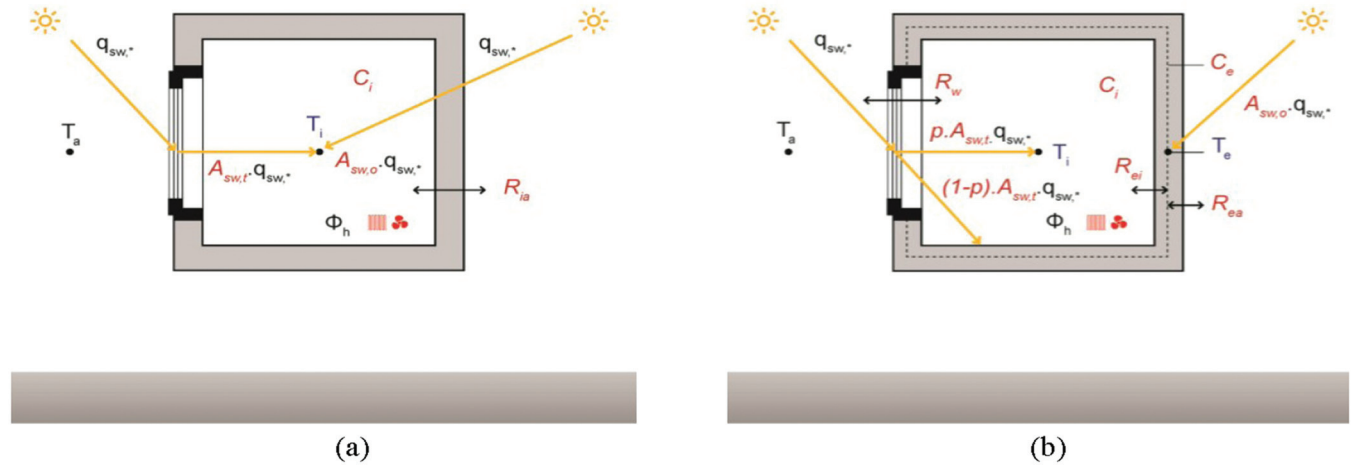

        (a)   (b)

Figure 3 *Diagrams of the assumed thermal models Ti (a) and TiTe (b). System states (indicated in blue): T_i [K] = indoor air temperature state; T_e [K] = envelope temperature state. Inputs (black): T_a [K] = outdoor air temperature; $q_{sw,*}$ [W/m²] = global solar radiation projection perpendicular to orientation $*$; Φ_h [W] = heating power. Estimated parameters (red): C_i and C_e [J/(kg·K)] = heat capacity associated with thermal nodes T_i and T_e, respectively; R_{ia}, R_{ei}, and R_{ea} [K/W] = thermal resistance between T_i – T_a, T_i – T_e, and T_e – T_a, respectively; R_w [K/W] = thermal resistance of window; $A_{sw,t}$ and $A_{sw,o}$ [m²·K] = fraction of solar radiation entering through transparent window area and opaque parts, respectively.*

tional state T_e [K] is considered between thermal nodes T_a and T_i, comprising the larger fraction C_e of the total heat capacity $C_i + C_e$ effectively charged or discharged during the experiment. R_{ei} and R_{ea} [K/W] represent the thermal resistances between $T_i - T_e$ and $T_e - T_a$, respectively.

Model TiTe.1

$$dT_i = \left(\frac{1}{C_i R_{ei}}(T_e - T_i) + \frac{\phi_h}{C_i} \right) dt + d\omega_i(t)$$

$$dT_e = \left(\frac{1}{C_e R_{ea}}(T_a - T_e) + \frac{1}{C_e R_{ei}}(T_i - T_e) \right) dt + d\omega_e(t)$$

(8)

Model TiTe.2

$$dT_i = \left(\frac{1}{C_i R_{ei}}(T_e - T_i) + \frac{\phi_h}{C_i} + \frac{p A_{sw,t} q_{sw,*}}{C_i} \right) dt + d\omega_i(t)$$

$$dT_e = \left(\begin{array}{c} \frac{1}{C_e R_{ea}}(T_a - T_e) + \frac{1}{C_e R_{ei}}(T_i - T_e) \\ + \frac{((1-p) A_{sw,t}) q_{sw,*} + A_{sw,o} q_{sw,*}}{C_e} \end{array} \right) dt + d\omega_e(t)$$

(9)

As a base case (Equation 8), model TiTe.1 does not consider solar radiation $q_{sw,*}$ as an input. Figure 3b and Equation 9 illustrate how the influence of the latter is modeled in model TiTe.2. A fraction p of the solar radiation entering the box through the south-facing window ($A_{sw,t} q_{sw,*}$) is considered to affect the indoor temperature state T_i directly. The other fraction $1 - p$ is expected to consequently strike the fabric components and influence the newly considered envelope state T_e. In addition, a small fraction $A_{sw,o}$ of solar radiation is expected to enter the state T_e through the opaque envelope surfaces.

To differentiate between the transparent and opaque components, the indoor air can be coupled directly with the ambient air (via R_w), without any associated heat capacity (Equation 10). This can be reasonably assumed due to the fact that the heat capacity of the window is likely to be negligible in comparison with the opaque fabric parts (Rabl 1988).

Model TiTe.3

$$dT_i = \left(\begin{array}{c} \frac{1}{C_i R_{ei}}(T_e - T_i) + \frac{1}{C_i R_w}(T_a - T_i) \\ + \frac{\phi_h}{C_i} + \frac{p A_{sw,t} q_{sw,*}}{C_i} \end{array} \right) dt + d\omega_i(t)$$

$$dT_e = \left(\begin{array}{c} \frac{1}{C_e R_{ea}}(T_a - T_e) + \frac{1}{C_e R_{ei}}(T_i - T_e) \\ + \frac{((1-p) A_{sw,t}) q_{sw,*} + A_{sw,o} q_{sw,*}}{C_e} \end{array} \right) dt + d\omega_e(t)$$

(10)

Model TiTeiTea

In a last step, a more sophisticated third-order model is considered by assuming two states T_{ei} and T_{ea} between thermal nodes T_a and T_i, as illustrated in Figure 4. This assumption is likely to be valid in many practical cases, e.g., when considering a dwelling with insulated walls, where the heat capacity is concentrated at either side of a light insulating layer.

C_{ei} and C_{ea} [J/(kg·K)] represent the heat capacities associated with T_{ei} and T_{ea}. R_{ei}, R_e, and R_{ea} [K/W] represent the thermal resistances between the respective thermal nodes T_i, T_{ei}, T_{ea}, and T_a. The fraction $1 - p$ of the solar radiation that enters the box through the window ($A_{sw,t} q_{sw,*}$) is assumed to affect the indoor fabric state T_{ei}, whereas the outdoor fabric state T_{ea} is independently affected ($A_{sw,o} q_{sw,*}$) by solar radiation striking the outside surface of the fabric.

With T_{ea} representing a state at the outer layers of the fabric, it becomes sensible to additionally inject this state with radiative heat exchange to the sky.

Hence, two three-order models are considered in the identification, only differing in the state equation for T_{ea}. Model TiTeiTea.1 is described by Equations 11–12. Model TiTeiTea.2 is governed by Equation 11 and the modified T_{ea} state equation in Equation 13, including the influence of longwave radiative heat exchange to the sky, governed by the radiative heat transfer coefficient f [W/K].

Model TiTeiTea

$$dT_i = \left(\frac{1}{C_i R_{ei}}(T_{ei} - T_i) + \frac{\phi_h}{C_i} + \frac{p A_{sw,t} q_{sw,*}}{C_i} \right) dt + d\omega_i(t)$$

$$dT_{ei} = \left(\begin{array}{c} \frac{1}{C_{ei} R_e}(T_{ea} - T_{ei}) + \frac{1}{C_{ei} R_{ei}}(T_i - T_{ei}) \\ + \frac{((1-p) A_{sw,t}) q_{sw,*}}{C_{ei}} \end{array} \right) dt + d\omega_{ei}(t)$$

(11)

Model TiTeiTea.1

$$dT_{ea} = \left(\begin{array}{c} \frac{1}{C_{ea} R_{ea}}(T_a - T_{ea}) \\ + \frac{1}{C_{ea} R_e}(T_{ei} - T_{ea}) + \frac{A_{sw,o} q_{sw,*}}{C_{ea}} \end{array} \right) dt + d\omega_{ea}(t)$$

(12)

Model TiTeiTea.2

$$dT_{ea} = \left(\begin{array}{c} \frac{1}{C_{ea} R_{ea}}(T_a - T_{ea}) \\ + \frac{1}{C_{ea} R_e}(T_{ei} - T_{ea}) + \frac{A_{sw,o} q_{sw,*}}{C_{ea}} \\ + \frac{f}{C_{ea}}(T_{sky} - T_{ea}) \end{array} \right) dt + d\omega_{ea}(t)$$
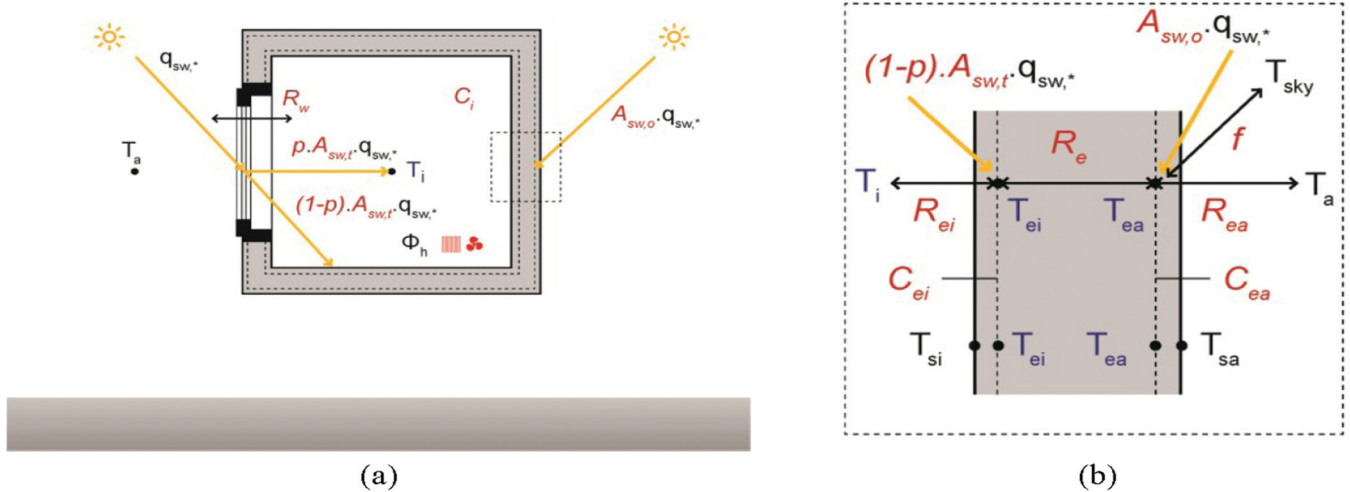
(13)

Figure 4 *Diagrams of model TiTeiTea: (a) overview of the considered heat dynamics and (b) detailed view of considered temperature states and assumed heat dynamics in the opaque fabric components. System states (indicated in blue): T_i [K] = indoor air temperature state; T_{ei} [K] = inner envelope temperature state; T_{ea} [K] = outer envelope temperature state. Inputs (black): T_a [K] = outdoor air temperature; $q_{sw,*}$ [W/m^2] = global solar radiation projection perpendicular to orientation *; Φ_h [W] = heating power; T_{sky} [K] = sky temperature. Estimated parameters (red): C_i, C_{ei}, and C_{ea} [J/(kg·K)] = heat capacity associated with thermal nodes T_i, T_{ei}, and T_{ea}, respectively; R_{ei}, R_e, and R_{ea} = thermal resistance between $T_i - T_{ei}$, $T_{ei} - T_{ea}$, and $T_{ea} - T_a$, respectively; R_w [K/W] = thermal resistance of window; $A_{sw,t}$ and $A_{sw,o}$ [m^2·K] = fraction of solar radiation entering through transparent window area and opaque parts, respectively; p [dimensionless] = fraction of solar radiation affecting T_i; f [W/K] = radiative heat transfer coefficient governing radiative heat exchange with sky.*

Model Selection Using Statistical Tests

The main aim of the modeling task is to retain a comprehensible model that effectively describes the thermal behavior of the investigated building in all its frequency parts.

The log-likelihood value associated with a certain candidate model (and given a certain data set) refers to the probability that the model actually has the observed response of the real system as a result. Evidently, the observed measurement data is more likely to result from well-performing models than from models of lower performance. To evaluate the descriptiveness of a certain model (alternative model) compared to that of a sub-model (null model), the likelihood ratio test is used. In addition to considering the log-likelihood values of respective models, it takes into account the number of estimated parameters.

The residuals constitute the difference between the modeled response and the actual measured response. Hence, the residuals associated with a suitable candidate thermal model should ideally show white noise behavior. A white noise signal represents a sequence of mutually uncorrelated, identically distributed random variables with zero mean and constant variance.

In a periodogram, the signal energy is decomposed into contributions relating to different frequencies. In the case of white noise, the residual periodogram should ideally vary around some constant. A cumulated periodogram plots the accumulation of a signal's energy contributions, hence depicting in which frequency range the model possibly tends to misrepresent the true thermal system's dynamic response. As the cumulated periodogram of theoretical white noise is a given, it offers a valuable tool to identify residual whiteness.

IDENTIFICATION OF SIMULATED BOX

In this section, the full set of identified models is discussed. The system identification is performed using CTSM-R, developed at DTU Informatics (DTU 2013). As a basis for the parameter estimation, the simulated measurement data are aggregated to 15 min averages. Tables 3, 4, and 5 collect the log-likelihoods for models Ti, TiTe, and TiTeiTea, respectively. The model complexity is gradually built up, with the final aim of obtaining a model of physical relevance, which has a complexity adapted to the investigated building and the data-embedded information.

Tables 3, 4, and 5 include *p*-values resulting from likelihood ratio tests. Here, the sub-model of lower complexity (lower model order or same model order with lower number of estimated parameters) that was seen to be most suitable in a previous step is assumed to be the null model, whereas the model to be evaluated is seen as the alternative. Hence, using a forward selection strategy, the most suitable model is retained from the set of candidate models defined in the previous section of this paper.

Table 3. Log-Likelihoods, Ti Models

	Ti.1	p-value	Ti.2	p-value	Ti.3
# Parameters	4		5		6
January	2048	$< 10^{-16}$	2783	1	2783
July	1487	$< 10^{-16}$	1867	1	1866

Table 4. Log-Likelihoods, TiTe Models

	p-value	TiTe.1	p-value	TiTe.2	p-value	TiTe.3
# Parameters		9		12		13
January	$< 10^{-16}$	2965	0.475	2966	0.742	2966
July	$< 10^{-16}$	1981	$< 10^{-16}$	2049	1	2047

Table 5. Log-Likelihoods, TiTeiTea Models

	p-value	TiTeiTea.1	p-value	TiTeiTea.2
# Parameters		16		17
January	0.845	2966	7.185e-12	2999
July	1.556e-12	2080	0.024	2082

For each model order (models Ti, TiTe, TiTeiTea), the best-performing models are indicated in grey in Tables 3, 4, and 5. The associated residuals and corresponding ACFs, both for winter and summer measurement campaigns, are shown in Figure 5. Figure 6 shows the log-likelihoods, and finally, Figure 7 depicts the respective cumulated periodograms of all considered candidate models.

Model Ti

Table 3 shows the log-likelihoods of models Ti.1, Ti.2, and Ti.3 and the p-values resulting from the likelihood ratio test statistic.

It is evident that the addition of the heating power signal Φ_h as an input (models Ti.2 and Ti.3) greatly increases the log-likelihood of the model. As seen in Figure 6, this represents the most important leap forward in the case of this model performance indicator. At the same time, the cumulative periodogram (Figure 7) shows that an important step is taken toward residual whiteness.

The addition of solar radiation as an input (model Ti.3), however, does not seem to yield an important improvement to the model fit. Intuitively, this seems plausible for the winter experiment, with little associated solar radiation. It is, however, confirmed by the results relating to the summer experiment. It is important to note that the global solar radiation perpendicular to a south-oriented vertical surface is selected as the sole solar radiation projection $q_{sw,*}$, serving as an input to the current and higher-order models.

The ACF of model Ti.2 shows a certain diurnal wave pattern for both winter and, above all, summer experiments. In the latter case, the peaks in the ACF are also clearly seen to cross the 5% confidence bands. Hence, model Ti.2 inadequately describes the output of the system. The wavy pattern and the important peaks indeed reveal that the model output T_i is partly dependent on earlier values of itself, whereas the model should explain the output as a function of the inputs and other eventual system states.

Model TiTe

As evident from the log-likelihoods and the p-value test statistics collected in Table 4 and plotted in Figure 6, the model description is greatly improved when extended by a capacitive thermal node between T_a and T_i. From the ACF (Figure 5) and the cumulated periodogram (Figure 7), the residuals are shown to exhibit white noise behavior for both winter and summer measurements. Hence, the model is able to adequately describe the investigated system in all its frequency components.

From the analysis of models Ti, it was seen that solar radiation does not necessarily represent a significant heat input when modeling the indoor temperature of the investigated KI Test Box. This is confirmed here for the winter experiments (model TiTe.2 vs. model TiTe.1). On the other hand, for the July experiment, $q_{sw,*}$ does serve as an important input to accurately describe the KI Test Box response. Hence, in the latter case, the most suitable model is model TiTe.2, whereas for the winter experiment model TiTe.1 represents the best option in the class of second-order candidate models.

For both measurement campaigns, modeling the transparent window component separately (model TiTe.3, Equation 10) does not yield a significant improvement. Hence, the low-capacitive window is no longer distinguished in models TiTeiTea.

Inspecting the ACF, the diurnal wave pattern seems to persist and become slightly more apparent in the case of the January experiment, whereas in the case of the July experiment it is seen to have been completely disentangled.

Model TiTeiTea

At first sight, the log-likelihoods of models TiTe and TiTeiTea (Figure 6, Tables 4 and 5) seem to suggest that the second-order models (models TiTe) already describe the thermal system with sufficient accuracy. However, the likelihood ratio test results in Table 5 clearly show that by adding another capacitive thermal node between T_a and T_i a significant improvement of the model is attained. Especially in the case of the summer experiment (models TiTe.2 to TiTeiTea.1 and TiTeiTea.1 to TiTeiTea.2), but the improvement from models TiTe.1 to TiTeiTea.2 in the case of the winter experiment is also seen to be significant.
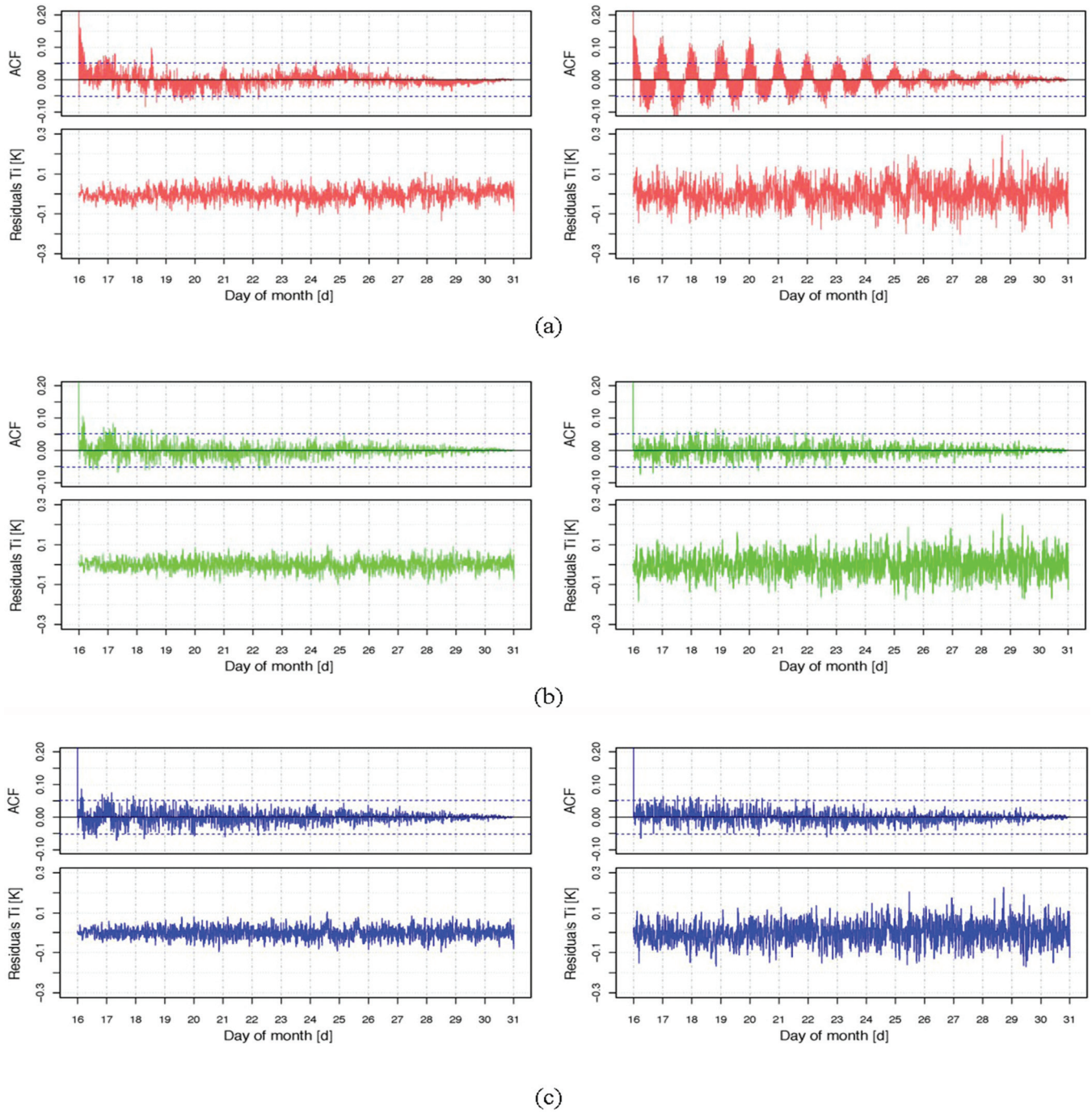
Figure 5 *Residual plots and corresponding ACFs for selected models, fitted to simulated measurement data collected in January 2011 (left) and in July 2011 (right), respectively: (a) residuals output T_i of model Ti.2, (b) residuals output T_i of model TiTe.1 for January and model TiTe.2 for July, and (c) residuals output T_i of model TiTeiTea.2. The stapled blue lines indicate a 5% confidence band.*
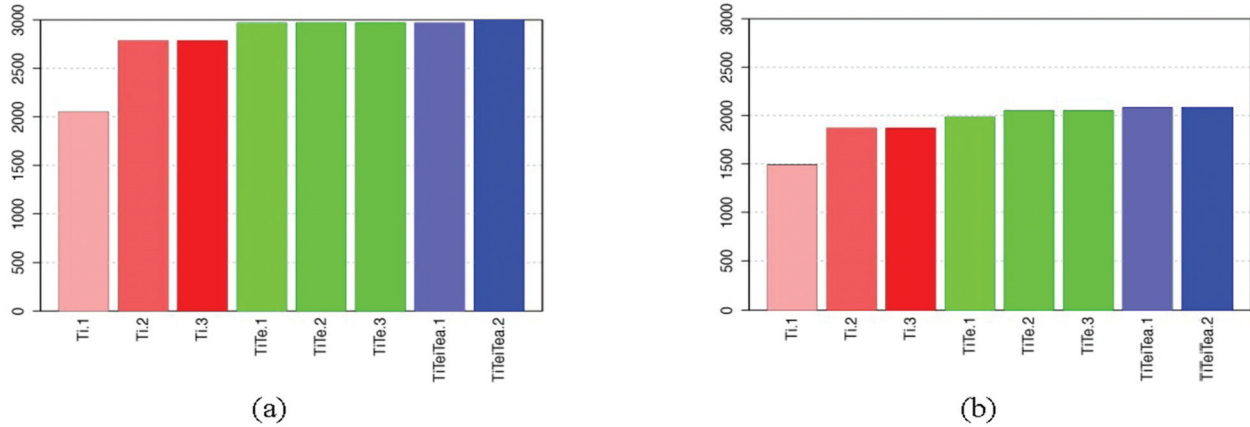
Figure 6 *Log-likelihoods of the considered candidate models, fitted to measurement data: (a) January 2011 and (b) July 2011.*
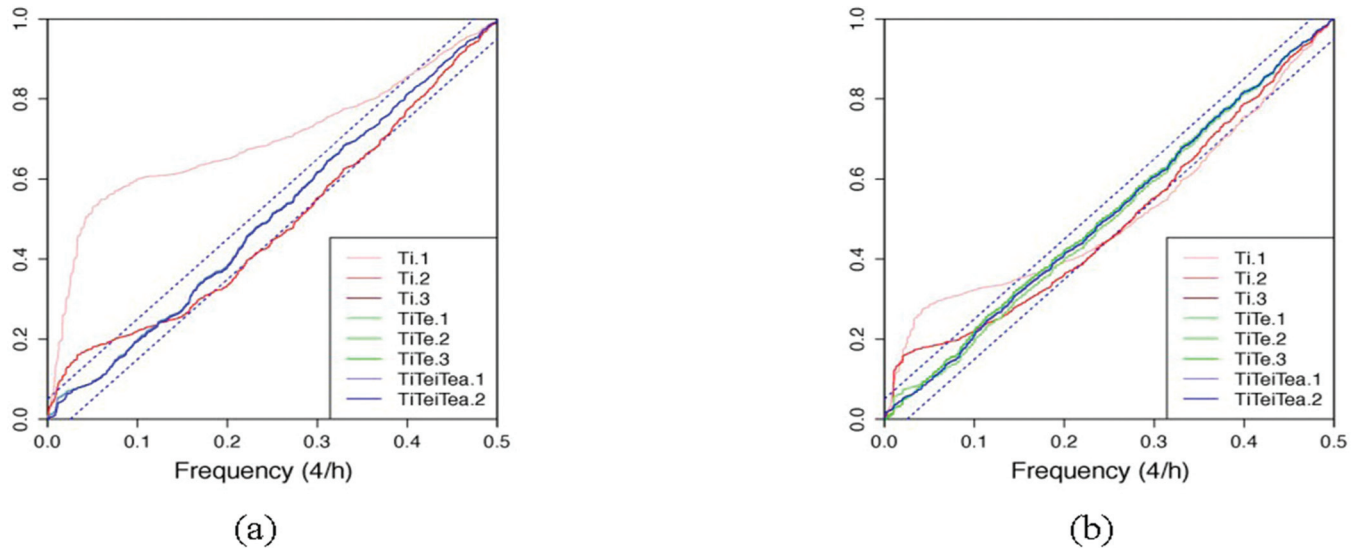

Figure 7 *Cumulated periodograms of the considered candidate models, fitted to measurement data: (a) January 2011 and (b) July 2011. Residual whiteness is apparent when the plotted line falls within the blue stapled bounds.*

In the case of the experiment in January, the model improvement TiTe.1 to TiTeiTea.1 is proven not to be significant. However, skipping a step and going from TiTe.1 to TiTeiTea.2 does prove to be a step forward in the modeling task (*p*-value: 7.185e-12). As expected from the outset, looking at the sky temperature time series in Figure 2b, the long-wave radiative heat exchange with the sky (the additional term in Equation 13) is seen to have an important influence on the KI Test Box behavior. This is confirmed by the log-likelihood of model TiTeiTea.2 and the likelihood ratio tests with TiTe.1 (January) and TiTe.2 (July) as null models and TiTeiTea.2 (January and July) as the alternative model (Table 5).

Cross-Validation of Identified Models

An important distinction needs to be made between the mere characterization of the building dynamics, the character-

ization of the thermal performance (e.g., *R* and *C*) of buildings, and the model-based prediction of its response to certain inputs or imposed boundary conditions. In this section, the predictive performance of the identified models is tested by simulating the KI Test Box response in another period than the period over which the model was trained—i.e., the models are cross-validated.

The root mean square errors plotted in Figures 8e and 8f confirm the third-order models perform best. Additionally, it is seen that the higher-order models identified on the basis of the summer experiment outperform the ones identified on the basis of the winter experiment when it comes to prediction. This is contrary to what might be expected from the log-likelihoods discussed previously. As illustrated by Figures 8b and 8d, the models trained using the January data set, although grasping the KI Test Box dynamics, have not learned to prop-
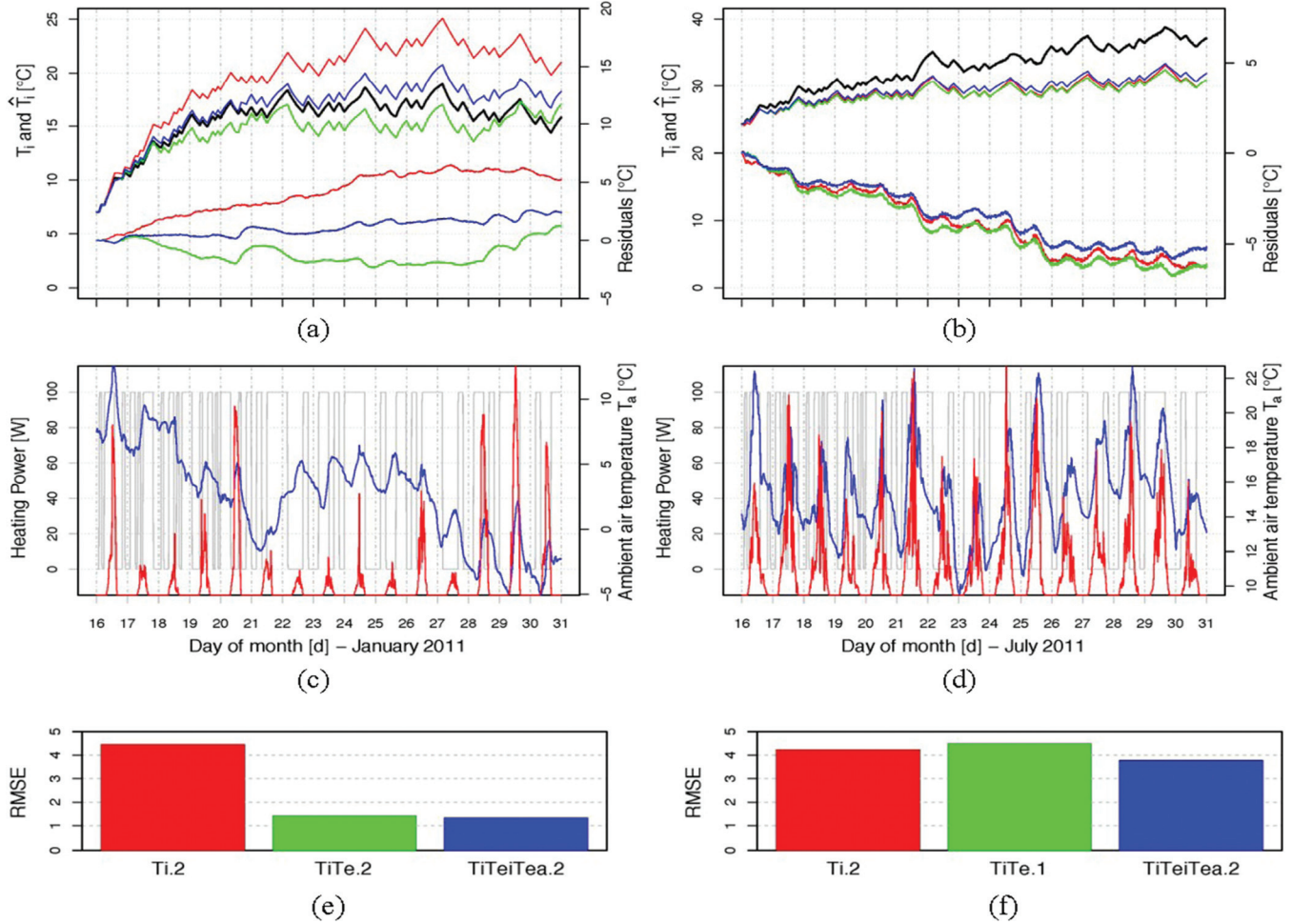
Figure 8 *(a) KI Test Box response simulated in January, using models Ti.2 (red), TiTe.2 (green), and TiTeiTea.2 (blue) identified on the basis of the July training data set; direct comparison with the actual measured response during the January experiment, complemented with residual plots. (b) KI Test Box response simulated in July, using models Ti.2 (red), TiTe.1 (green), and TiTeiTea.2 (blue) identified on the basis of the January training data set; direct comparison with the actual measured response during the July experiment, complemented with residual plots. (c) Ambient air temperature T_a [K], PRBS as heating power Φ_h [W], and global solar radiation on a vertical south-oriented wall $q_{sw,south}$ [W/m²] during January experiment. (d) Ambient air temperature T_a [K], PRBS as heating power Φ_h [W], and global solar radiation on a vertical south-oriented wall $q_{sw,south}$ [W/m²] during July experiment. (e) and (f) Root mean square errors.*

erly cope with the heat input to the indoor environment due to solar radiation. This is likely to be attributed to both the limited window surface of the KI Test Box and the fact that the solar irradiance is rather low during the winter experiment. The actual solar gain is seen to be underestimated, which is revealed by the steady overall increase of the absolute residual values with simulation time, as well as the modest reductions followed by steep rises in the absolute residual values during each day with considerable solar radiation.

CONCLUSIONS

The aim of this research was to investigate the ability to identify the thermal dynamics of buildings using grey-box modeling. In this framework, simplified thermal dynamic models were defined based on prior physical knowledge. These models were consecutively fitted to *simulated* data sets acquired from *simulated* experiments performed on a *simulated* small scale model of a building, the KI Test Box of IEA ECBCS Annex 58 (Roels 2011). The performance of the fitted models was compared using well-known statistical tests. The identified thermal dynamic models can be used to characterize the actual thermal performance of buildings and to simulate its response to boundary conditions to which it might be subdued.

In general, it is seen to be crucial to inspect both the log-likelihoods and the likelihood ratio test when judging whether an alternative (more complex) model actually performs better.

The main aim of the modeling task is to obtain a model with associated residuals exhibiting white noise characteristics. Residual whiteness becomes apparent in the auto-correlation function (ACF) plot and the cumulated periodograms.

The order of the candidate models found to be most suitable depends on the perceivable or apparent time constants of the investigated building. In other words, the time constants associated with the model reflect the accessible heat capacity that is effectively excited during the experiment. Whereas the accessibility of the thermal mass is solely determined by the composition of the building fabric, the effectively charged/discharged part additionally depends on the imposed experiment (T_i, Φ_h) and the outside weather conditions (T_a and $q_{sw,*}$, among others).

The simulated measurement campaigns in winter are seen to systematically yield better model fits. The standard deviation of the residuals is considerably smaller than its counterparts associated with models fit to measurement data in summer. Model fits for both winter and summer experiments show residual whiteness as soon as two or more states are considered (models TiTe and TiTeiTea). In the case of the second-order TiTe models, it is seen that the most suitable model for the winter and summer experiments differs, even though the imposed experiments are identical. This clearly illustrates that, aside from the investigated building and the imposed experiment (heating power signal Φ_h, e.g., PRBS), the most suitable model depends on the particular weather conditions (T_a, $q_{sw,*}$, etc.) taking place during the experiment. The latter effectively excite the building in their respective prevalent frequency components. In order to obtain reliable and separated parameter estimates, however, a heating power signal that is uncorrelated with the outside weather conditions, persistently exciting the building, is required.

Although the summer experiment yields model fits with lower log-likelihoods than the winter experiment, it is seen to deliver models that are better able to simulate the KI Test Box response in other circumstances than over which they were fitted. Cross-validation clearly shows that the solar gains are not properly modeled when models are trained on measurement data in January.

Influential weather conditions need to be accounted for in a suitable way. Taking into account solar radiation, however significant in the higher-order models, is seen to only modestly improve the quality of the model fit. The limited surface area of the KI Test Box window partly serves to explain this. Additionally, as illustrated by the results for the winter experiment, the intensity of the solar radiation input signal will partly determine its significance.

All solar radiation projections could potentially serve as input to the models. As opposed to model Ti.3, the choice of the solar radiation projection that serves as input to models TiTe.2, TiTe.3, TiTeiTea.1, and TiTeiTea.2 becomes less straightforward. Future research should investigate the possibility to sensibly relate different solar radiation projections to different thermal nodes considered in the system, or how to take into account different projections depending on the time of day.

The KI Test Box was simulated to be perfectly airtight. Hence, the wind speed and direction are not influential. Their influence on the convective heat transfer coefficient hence is negligible, given the fact that the KI Test Box is relatively well insulated.

It is important to note that all of the models considered in this paper are linear time-invariant models, whereas the thermal behaviour of the real system is essentially nonlinear, due to such factors as radiative heat exchange with sky, dependence of thermal resistance of building fabric on temperature, influence of solar radiation, and dependence of convective heat transfer coefficients on wind speed and direction. Nonetheless, it is seen that good fits are attained and reasonable characterizations are within reach. This greatly depends, however, on the thermal performance of the investigated building, the weather conditions, the imposed experiment, and its purpose.

NOMENCLATURE

λ	=	shortest time period at which the heating power (PRBS) shifts from one level to the other, h
R	=	thermal resistance, K/W
C	=	heat capacity, J/(kg·K)
A	=	solar aperture, m²·K
T	=	absolute temperature, K
θ	=	temperature, °C
Φ	=	power, W
q	=	heat flux, W/m²
p	=	fraction of solar radiation entering T_i, dimensionless
f	=	radiative heat transfer coefficient (radiative heat exchange with sky), W/K
α	=	solar absorption factor, dimensionless
ω	=	process noise, K
ε	=	measurement noise, K
ξ	=	emissivity, dimensionless
τ	=	time constant, s

Subscripts

i	=	indoor environment
a	=	ambient/outdoor environment
e	=	envelope
ei	=	inside of the envelope
ea	=	outside of the envelope
g	=	ground
h	=	heating
sw	=	shortwave
ir	=	infrared
c	=	convective

t	=	transparent
o	=	opaque
sky	=	sky
w	=	window
*	=	projection perpendicular to horizontal, north-, east-, south-, and west-oriented surfaces
k	=	discrete time step

REFERENCES

Bacher, P., and H. Madsen. 2011. Identifying suitable models for the heat dynamics of buildings. *Energy and Buildings* 43:1511–22.

Bell, M., J. Wingfield, and D. Miles-Shenton. 2010. Low carbon housing. Lessons from Elm Tree Mews. Joseph Rowntree Foundation.

DTU. 2013. CTSM-R. Software used for parameter estimation: Implementation of the Continuous Time Stochastic Modeling (CTSM) software in R. DTU Informatik, Denmark. www.ctsm.info

Godfrey, K.R. 1980. Correlation methods. *Automatica* 16(5): 527–34.

Hens, H., A. Janssens, W. Depraetere, J. Carmeliet, and L. Lecompte. 2007. Brick cavity walls: A performance analysis based on measurements and simulations. *Journal of Building Physics* 31(2):95–124.

Kristensen, N.R., and H. Madsen. 2003. *Continuous Time Stochastic Modelling. CTSM 2.3—Mathematics Guide.* Denmark: DTU Informatik.

Lowe, R.J., et al. 2007. Evidence for heat losses via party wall cavities in masonry construction. *Building Service Engineers Research and Technology* 28(2):161–81.

Madsen, H., and J.M. Schultz. 1993. Short time determination of the heat dynamics of buildings. Technical report, DTU Informatik, Denmark.

Muneer, T. 1989. Algorithms for estimating hourly solar irradiation on slopes. *Building Serv. Eng. Res. Technol.* 10(2):81–83

Rabl, A. 1988. Parameter estimation in buildings: Methods for dynamic analysis of measured energy use. *Journal of Solar Energy Engineering—Transactions of the ASME* 110(1):52–66.

Reda, I., and A. Andreas. 2008. Solar Position Algorithm for Solar Radiation Applications, NREL Report No. TP-560-34302; 2003, revised January 2008. Golden, CO: National Renewable Energy Laboratory.

Roels, S. 2011. Reliable building energy performance characterisation based on full scale dynamic measurements. Annex text, November 2011. www.kuleuven.be/bwf/projects/annex58/index.htm

Thyregod, P., and H. Madsen. 2006. *General and Generalized Linear Models*. Lyngby, Denmark: IMM, DTU Informatik.

Physibel. 2011. VOLTRA version 7.0w. Software used for simulations. Physibel, Maldegem, Belgium.